Report

Current Biology

Visual boundary cues suffice to anchor place and grid cells in virtual reality

Highlights

- Elevated (but not flat) visual boundaries anchor spatial firing in virtual reality
- Unstable grid cells exhibit hexagonal patterns on short (5 s) timescales
- Invisible boundaries (inferred from a beacon cue) partly stabilize place fields
- A subset of place cells shows allocentric directional tuning toward reward locations

Authors

Xiuting Yang, Francesca Cacucci, Neil Burgess, Thomas Joseph Wills, Guifen Chen

Correspondence

t.wills@ucl.ac.uk (T.J.W.), guifen.chen@qmul.ac.uk (G.C.)

In brief

Yang et al. show visual cues from elevated walls are necessary for stable place and grid cell firing in virtual reality, whereas cues from a patterned floor are not. Without visible boundaries, grid cells show hexagonal patterns only on short timescales. Invisible boundaries (inferred from beacon cue movement) partly stabilize nearby place fields.

Yang et al., 2024, Current Biology *34*, 1–9
May 20, 2024
https://doi.org/10.1016/j.cub.2024.04.026

CellPress

Current Biology

CellPress
OPEN ACCESS

Report

Visual boundary cues suffice to anchor place and grid cells in virtual reality

Xiuting Yang,[1] Francesca Cacucci,[2] Neil Burgess,[3,4] Thomas Joseph Wills,[5,6,*] and Guifen Chen[1,6,7,8,*]
[1]School of Biological and Behavioural Sciences, Queen Mary University of London, 327 Mile End Road, London E1 4NS, UK
[2]Department of Neuroscience, Physiology, and Pharmacology, University College London, Gower Street, London WC1E 6BT, UK
[3]Institute of Cognitive Neuroscience, University College London, 17 Queen Square, London WC1N 3AZ, UK
[4]Queen Square Institute of Neurology, University College London, Queen Square, London WC1N 3BG, UK
[5]Department of Cell and Developmental Biology, University College London, Gower Street, London WC1E 6BT, UK
[6]Senior author
[7]X (formerly Twitter): @GuifenChen
[8]Lead contact
*Correspondence: t.wills@ucl.ac.uk (T.J.W.), guifen.chen@qmul.ac.uk (G.C.)
https://doi.org/10.1016/j.cub.2024.04.026

SUMMARY

The hippocampal formation contains neurons responsive to an animal's current location and orientation, which together provide the organism with a neural map of space.[1–3] Spatially tuned neurons rely on external landmark cues and internally generated movement information to estimate position.[4,5] An important class of landmark cue are the boundaries delimiting an environment, which can define place cell field position[6,7] and stabilize grid cell firing.[8] However, the precise nature of the sensory information used to detect boundaries remains unknown. We used 2-dimensional virtual reality (VR)[9] to show that visual cues from elevated walls surrounding the environment are both sufficient and necessary to stabilize place and grid cell responses in VR, when only visual and self-motion cues are available. By contrast, flat boundaries formed by the edges of a textured floor did not stabilize place and grid cells, indicating only specific forms of visual boundary stabilize hippocampal spatial firing. Unstable grid cells retain internally coherent, hexagonally arranged firing fields, but these fields "drift" with respect to the virtual environment over periods >5 s. Optic flow from a virtual floor does not slow drift dynamics, emphasizing the importance of boundary-related visual information. Surprisingly, place fields are more stable close to boundaries even with floor and wall cues removed, suggesting invisible boundaries are inferred using the motion of a discrete, separate cue (a beacon signaling reward location). Subsets of place cells show allocentric directional tuning toward the beacon, with strength of tuning correlating with place field stability when boundaries are removed.

RESULTS

Place and grid cells were recorded while mice navigated in a 2-dimensional (2D) virtual reality environment[9] (796 place cells and 138 grid cells; see Data S1A for breakdown by animal and experimental session and Figure S1A for details of apparatus). The external sensory cues defining the environment were purely visual, while the animal's movement around the environment was coupled to its movement on a spherical trackball. Mice were trained to navigate toward a moveable beacon to receive a reward.[9] After mice had learned this task,[9] we tested the necessity of different visual cues for place and grid cell firing by removing specific subsets of these cues as mice continued to perform the navigation task (Figure S1A; see details in STAR Methods).

Removing the wall cues alone produced a strong disruption in the spatial specificity and within-trial (intra-trial) stability of place cells, as did removing both walls and floor cues simultaneously (Figures 1B–1F). By contrast, removing only floor cues had no significant effect on place cell spatial firing (Figures 1A and 1F). Removing the floor cues only did, however, cause a modest degree of remapping, as measured by the across-trial (inter-trial) stability of place cell firing between the cue-present and cue-absent trials (Figures 1A and 1F). This indicates a degree of saliency of floor cues to place cell firing, but only the removal of wall cues resulted in a significant decrease in place cell within-trial stability and spatial tuning.

The effects of cue removal on grid cells paralleled those observed for place cells: removing walls only or floor and walls together resulted in a strong reduction in gridness scores and within-trial stability, while there was no significant effect of removing the floor cues alone (Figures 1A–1C, 1G, and 1H). Unlike place cells, grid cells did not significantly remap between cue-present and floor-off trials (Figure 1I). Analyzing grid cell data using simultaneously recorded grid module ensembles as statistical units did not alter the reported results (Figures 1J–1L).

Furthermore, the walls-off condition disrupted place and grid cell firing to the same extent as the all-off condition: there were no significant differences in spatial information, gridness scores, or intra-trial stability between these conditions (Figures 1D, 1E,

Please cite this article in press as: Yang et al., Visual boundary cues suffice to anchor place and grid cells in virtual reality, Current Biology (2024), https://doi.org/10.1016/j.cub.2024.04.026

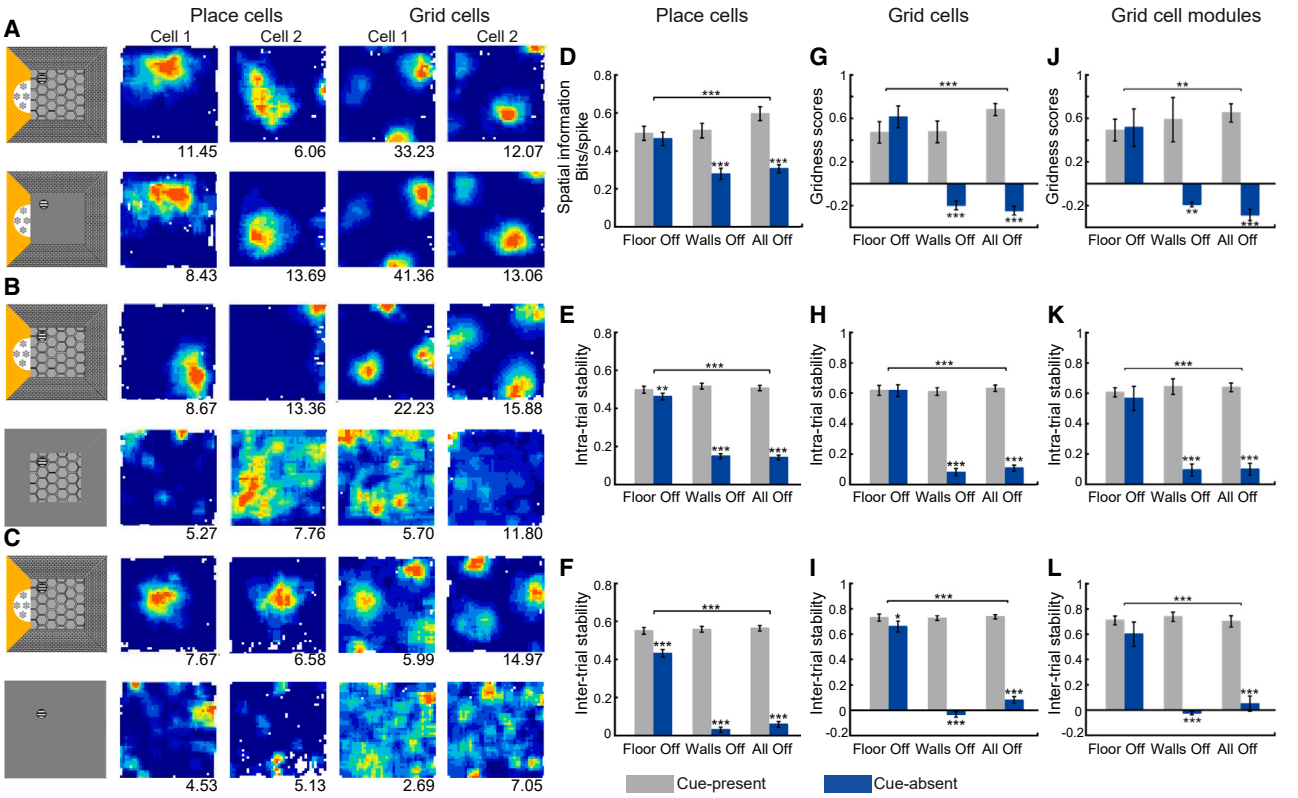

Figure 1. Visual cues from boundaries provide sufficient inputs to stabilize spatial patterns of place cells and grid cells

(A) Visual cues were removed from the floor (floor off).

(B) Visual cues were removed from all four walls (walls off).

(C) All environmental visual cues were removed (all off). The panels on the left column are schematic of the manipulations with a cue-present environment on the top and a cue-absent environment on the bottom, the 2nd and 3rd columns are the rate maps of two example place cells in the corresponding environments, and the 4th and 5th columns are rate maps of two example grid cells. Numbers at the bottom right of rate maps are peak firing rates (Hz).

(D–I) Comparison of firing properties of place cells and grid cells in all three manipulations including spatial information (D; ANOVA cue presence*manipulation, $F(2,617) = 26.94$, $p < 0.001$; simple main effects [SME] cue present versus absent, floor off, $p = 0.305$; walls off, $p < 0.001$; all off, $p < 0.001$), intra-trial stability (E; ANOVA cue presence*manipulation, $F(2,617) = 90.36$, $p < 0.001$; SME absent versus present, floor off, $p < 0.01$; walls off, $p < 0.001$; all off, $p < 0.001$), and inter-trial stability between the cue-present and cue-absent trials (F; ANOVA cue presence*manipulation, $F(2,617) = 114.60$, $p < 0.001$; SME absent versus present, floor off, $p < 0.001$; walls off, $p < 0.001$; all off, $p < 0.001$) for place cells and gridness scores (G; ANOVA cue presence*manipulation, $F(2,109) = 32.92$, $p < 0.001$; SME absent versus present, floor off, $p = 0.202$; walls off, $p < 0.001$; all off, $p < 0.001$), intra-trial stability (H; ANOVA cue presence*manipulation, $F(2,109) = 64.45$, $p < 0.001$; SME absent versus present, floor off, $p = 0.972$; walls off, $p < 0.001$; all off, $p < 0.001$), and inter-trial stability (I; ANOVA cue presence*manipulation, $F(2,109) = 99.92$, $p < 0.001$; SME absent versus present, floor off, $p < 0.05$; walls off, $p < 0.001$; all off, $p < 0.001$) for grid cells. $^{**}p < 0.01$; $^{***}p < 0.001$.

(J–L) Re-analysis of the grid cell data, using the mean scores across all grids in a simultaneously recorded module as the statistical unit of analysis. Removing walls only or floor and walls together resulted in a strong reduction in gridness scores and intra- and inter-trial stability, while there was no significant effect of removing the floor cues alone.

(J) Gridness score: ANOVA cue presence*manipulation, $F(2, 11) = 12.45$, $p < 0.01$; SME absent versus present, floor off, $p = 0.874$; walls off, $p < 0.01$; all off, $p < 0.001$.

(K) Intra-trial stability between the cue-present and cue-absent trials: ANOVA cue presence*manipulation, $F(2, 11) = 29.12$, $p < 0.001$; SME absent versus present, floor off, $p = 0.484$; walls off, $p < 0.001$; all off, $p < 0.001$.

(L) Inter-trial stability between the cue-present and cue-absent trials: ANOVA cue presence*manipulation, $F(2, 11) = 25.03$, $p < 0.001$; SME absent versus present, floor off, $p = 0.154$; walls off, $p < 0.001$; all off, $p < 0.001$. $^{*}p < 0.05$; $^{**}p < 0.01$; $^{***}p < 0.001$.

See also Figure S1 and Data S1.

1G, and 1H). These results suggest that environmental walls are the cues responsible for stabilizing place and grid cell firing within this virtual environment.

A subset of cells was also recorded in a second cue-present trial, directly after the cue-absent trial. Both place and grid cells restored their firing patterns after visual cues were replaced, with the second cue-present trial showing significantly greater spatial information, gridness scores, and intra-trial stability than the cue-absent trial (Figures S1D–S1K). There were no significant differences in running speed between cue-present and cue-absent trials across all manipulations (Figure S1B). Mice collected a similar (floor-off) or slightly higher (walls-off, all-off) number of rewards in the cue-absent trials (Figure S1C). Place and grid cell spatial firing was disrupted even when these neurons were co-recorded with medial entorhinal cortex head direction cells (mEC HDCs) that retained their directional tuning in cue removal

Please cite this article in press as: Yang et al., Visual boundary cues suffice to anchor place and grid cells in virtual reality, Current Biology (2024), https://doi.org/10.1016/j.cub.2024.04.026

trials (Figures S1L–S1U). The above results confirm that disrupted firing in the cue-absent trial is a specific effect of visual cue removal, rather than the result of electrode instability over the experimental session, mouse behavior, or unstable heading information.

Computational models predict that grid cells can generate regular hexagonal patterns from purely idiothetic information.[10–13] Anchoring these patterns to the external world using landmark cues is thought to prevent instability arising from accrued path integration error.[14] We tested whether grid patterns were present at short timescales in the cue-absent conditions (walls-off and all-off), as this would be an indication of path integration drift. Time-windowed auto-correlogram firing rate maps (STAR Methods) showed hexagonal patterns at short time intervals (Figures 2A and 2B; peaking at 5 s), with progressive disruption at longer durations. Gridness scores of the time-windowed rate maps increased at longer durations when cues were present but decreased at longer durations when cues were absent (Figure 2C). Thus, hexagonal grid firing patterns were detectable over short time intervals in both cue-absent conditions. Similar results were observed using simultaneously recorded grid cell modules as statistical units of analysis (Figure 2E).

Optic flow is thought to be an important source of movement information that can contribute to path integration.[15,16] However, the patterned visual information provided by the floor did not significantly improve the gridness score at short timescales (Figures 2D and 2F). There was no evidence, therefore, that optic flow from patterned visual information supports grid cell stability in the virtual reality environment.

To investigate whether grid drift is primarily translational or directional, we constructed time-windowed cross-correlogram maps between simultaneously recorded grid cell pairs and tested whether directional offsets between grids are preserved at short timescales. We found that the change in directional offsets between cue-present and cue-absent (in a 5 s time window) was no greater than that between repeated cue-present trials, indicating that the directional component of grid firing was stable in cue-absent trials (Figure S2). This analysis further confirms (along with the stability of mEC HDCs) that cue removal in virtual reality leads to disruption of 2D spatial firing, despite the preservation of the head direction signal.

As the reward beacon was the only source of positional information in the all-off condition (STAR Methods), we reasoned that the mouse may infer the presence of the virtual boundary from the motion of the reward beacon relative to its own motor output. We tested whether such inferred boundaries could contribute to spatial firing stability in the all-off condition by calculating the intra-trial stability in separate boundary and center zones (STAR Methods). We found that cue removal consistently reduced stability in the center zone, relative to the boundary zone, for both place cells (Figure 3C) and grid cells (Figure 3D). However, the specific effects of cue removal were different across the two cell types. Place cells were equally stable across environmental boundary and center when cues were present but were significantly more stable near boundaries in the all-off condition (Figure 3C). These results suggest that, in a highly familiar environment, place fields can be at least partially stabilized by boundary cues even when these cues themselves are not perceptually available but are rather inferred from the movement (relative to motor output) of other, perceptually available, cues. Grid cells, by contrast, were more stable in the environment center when cues were present but became equally unstable at all environmental locations in the all-off condition (Figure 3D). This pattern of results was replicated in the subset of animals for which grid and place cells were simultaneously recorded (Figure 3E), ruling out across-animal sampling bias as a cause for this result. Taken together, these data indicate that place, but not grid representations, might benefit from the presence of the moving reward beacons to calculate location.

Our finding of higher grid field stability in the environment center, in the cue-present condition, has not previously been reported in real-world studies, raising the possibility that this phenomenon is specific to virtual reality. However, analysis of grid cells from the same cohort of mice recorded in real-world arenas revealed a similar result (albeit with a smaller effect size) (Figures S3G and S3H), even after controlling for positional sampling bias (Figures S3A–S3F, S3I, and S3J).

Following our unexpected finding that place fields can be stabilized by a boundary inferred from the movement of a discrete cue (the reward beacon), we tested whether place cell firing may be modulated by this cue. Specifically, we tested whether place cells encoded the animal's bearing to the reward beacon, irrespective of the animal's head orientation. In the baseline (cue present) condition, 18.6% (114/614) of place cells showed significant directional tuning toward the reward beacons (STAR Methods) (Figures 4A–4C). Directional tuning toward the beacon was reduced in the all-off condition (Figure 4D), but there remained a correlation between the degree of beacon tuning in baseline and all-off trials (Figure 4E), suggesting that beacon tuning is a cell-specific property. Moreover, the strength of place cells' allocentric tuning (Rayleigh vector scores) in the all-off condition was significantly and positively correlated with the intra-trial stability in the all-off condition, irrespective of the relative position of place fields with respect to environmental boundaries (Figure 4F), indicating that, in our experimental paradigm, the reward beacons help to stabilize the firing patterns of place cells in the all-off condition. We also tested whether place cell or grid cell firing was tuned to the reward position in 2D (x,y) space; however, we found no more tuning to the reward beacon than expected by chance (Figure S4). Furthermore, we did not find any correlation between the directional reward tuning of place cells and animals' performance on the reward beacon task (Figures 4G and 4H).

DISCUSSION

The hippocampus uses multimodal sensory information to generate spatially tuned neural firing and support spatial cognition.[17–22] Disentangling the contribution of different sensory modalities can be practically difficult in a real-world setting; hence the importance of introducing virtual reality techniques,[5,9,23,24] which allow arbitrary manipulations of sensory stimuli. We have shown that, in virtual reality, purely visual barriers, which present no somatosensory or olfactory cues to the animal (unlike real-world barriers), nonetheless support place and grid cell firing. Our results are consistent with previous evidence demonstrating the importance of boundaries for neural representations

Please cite this article in press as: Yang et al., Visual boundary cues suffice to anchor place and grid cells in virtual reality, Current Biology (2024), https://doi.org/10.1016/j.cub.2024.04.026

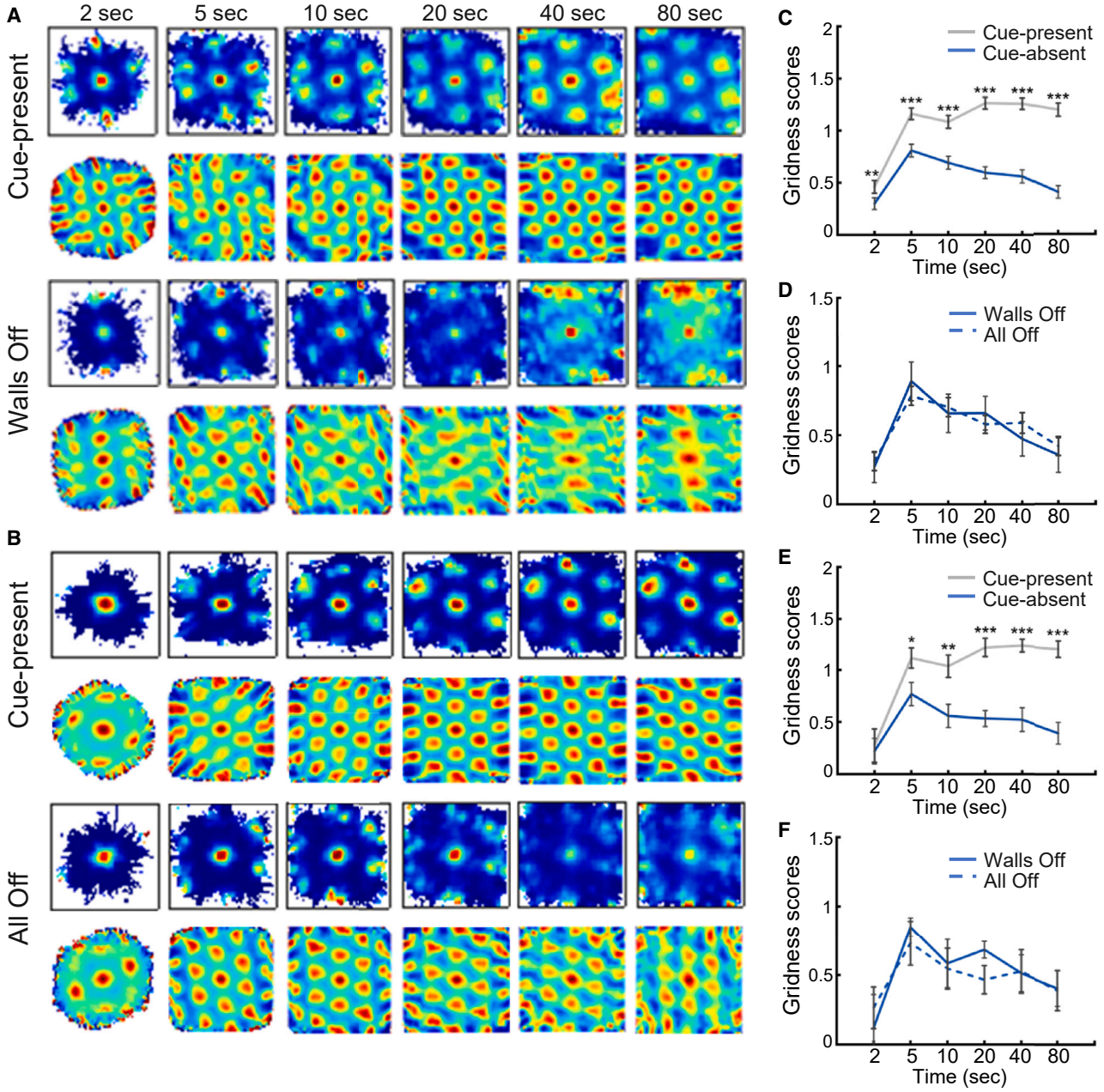

Figure 2. Grid cells maintain hexagonal patterns on short timescales

(A and B) Time-windowed rate maps and their auto-correlograms with 2, 5, 10, 20, 40, and 80 s windows of representative grid cells in cue-present (top rows) and cue-absent (bottom rows) for the walls-off (A) and all-off (B) conditions.

(C) Mean (±SEM) elliptical gridness scores calculated from the time-windowed displacement firing rate maps comparing cue-present (gray) with cue-absent (blue) trials. Two-way ANOVA duration-cue presence: SME duration $F(5, 136) = 37.34$, $p < 0.001$; interaction duration*cue presence $F(5,136) = 13.87$, $p < 0.001$.

(D) Mean (±SEM) elliptical gridness scores calculated from the time-windowed displacement firing rate maps comparing the walls-off (solid) with the all-off (dotted) conditions. Two-way ANOVA manipulation-duration: main effect of manipulation (walls off versus all off), $F(5, 135) = 0.02$, $p = 0.904$.

(E) Mean (±SEM) elliptical gridness scores calculated from the time-windowed displacement firing rate maps comparing cue-present (blue) with cue-absent (gray) trials with grid module as the statistical unit of analysis. Two-way ANOVA duration-cue presence: SME duration $F(5, 8) = 15.67$, $p < 0.001$; interaction duration*cue presence $F(5, 8) = 8.11$, $p < 0.001$.

(F) Mean (±SEM) elliptical gridness scores calculated from the time-windowed displacement firing rate maps comparing the walls-off (solid) with the all-off (dotted) conditions with grid module as the statistical unit of analysis. Two-way ANOVA manipulation-duration: main effect of manipulation (walls off versus all off), $F(5, 7) = 0.04$, $p = 0.800$. *$p < 0.05$; **$p < 0.01$; ***$p < 0.001$.

See also Figure S2.

Please cite this article in press as: Yang et al., Visual boundary cues suffice to anchor place and grid cells in virtual reality, Current Biology (2024), https://doi.org/10.1016/j.cub.2024.04.026

CellPress
OPEN ACCESS

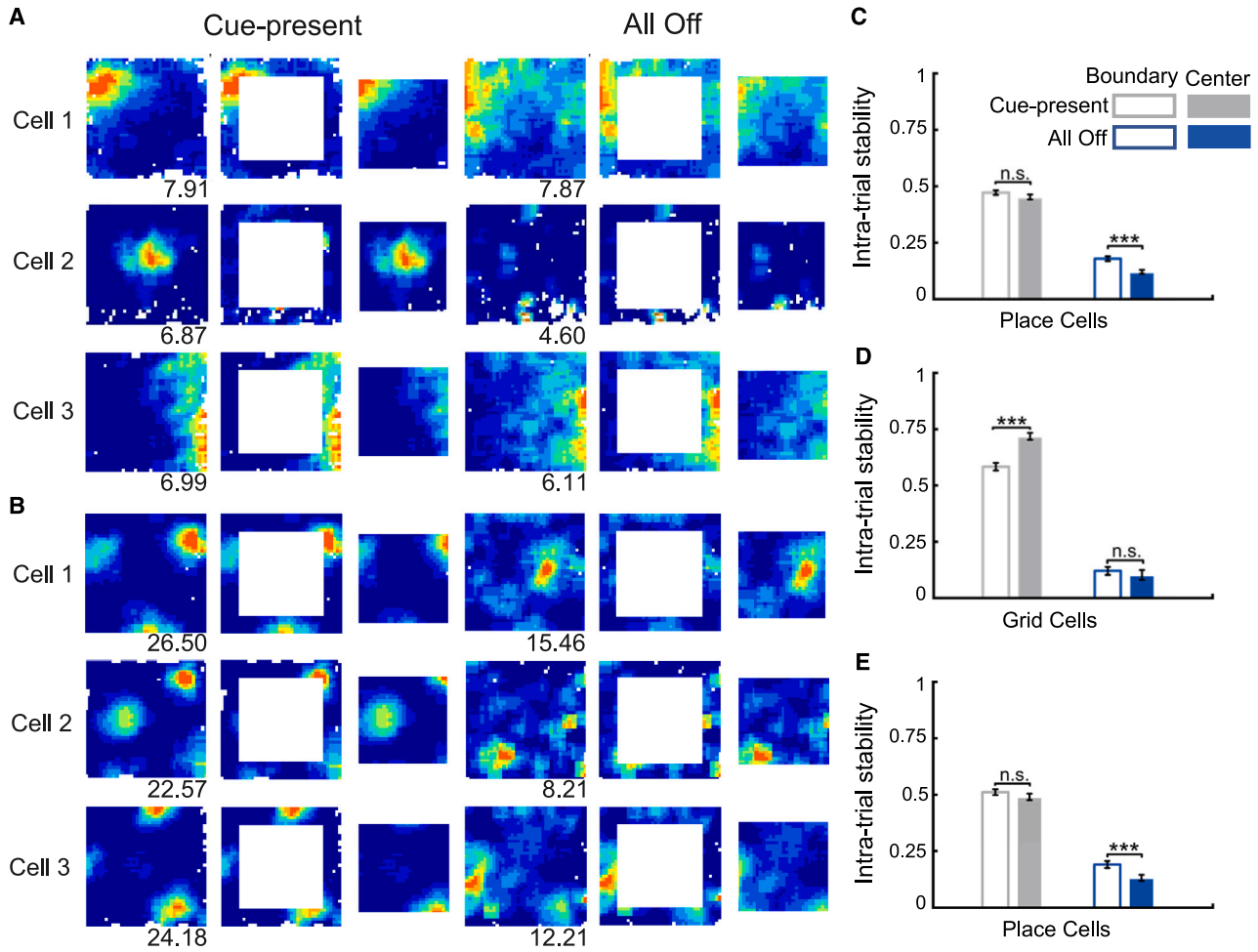

Figure 3. Proximity to inferred boundaries increases stability for both place cells and grid cells

(A) Rate maps of three example place cells recorded in a 60 cm virtual square in the cue-present and cue-absent (all-off) conditions.

(B) Rate maps of three example grid cells recorded in a 60 cm virtual square in the cue-present and all-off conditions. The left column shows the rate maps for the whole environment, the middle column shows the boundary area of the maps, and the right column shows the central area of the maps. Numbers at the bottom right of firing rate maps are peak firing rate (Hz).

(C) Intra-trial stability of boundary (open bars) and central (solid bars) rate maps in the cue-present (gray) and all-off (blue) conditions for place cells. ANOVA, zone*cue presence, $F(1,611) = 6.97$, $p < 0.01$. Paired t test: all off, $t(613) = 6.03$, $p < 0.001$; cue-present, $t(613) = 1.96$, $p = 0.051$.

(D) Intra-trial stability of boundary (open bars) and central (solid bars) rate maps in the cue-present (gray) and all-off (blue) conditions for grid cells. ANOVA, zone*cue presence, $F(1,106) = 34.97$, $p < 0.001$. Paired t test: all off, $t(106) = 0.85$, $p = 0.400$; cue-present, $t(106) = -8.41$, $p < 0.001$.

(E) Intra-trial stability of boundary (open bars) and central (solid bars) place fields in the cue-present (gray) and all-off (blue) conditions for the subset of place cells simultaneously recorded with grid cells. As for the full place cell dataset, place fields are equally stable across boundary and center zones in the cue-present condition and were significantly more stable near the boundary in the all-off condition. ANOVA, zone*cue presence, $F(1,317) = 4.26$, $p < 0.05$. Paired t test: all off, $t(317) = 4.65$, $p < 0.001$; cue-present, $t(317) = 1.56$, $p = 0.120$. ***$p < 0.001$.

See also Figure S3.

of space: boundaries shape firing patterns of place cells and grid cells in rodents,[6–8,25,26] as well as neural representations in the human medial temporal lobes.[27]

In the walls-off condition, a visual boundary is available to the animal in the form of the edge of the patterned floor texture, but this cannot support stable place and grid cell firing. Our results, thus, show for the first time that purely visual boundaries need to take a specific form, i.e., an elevated, not flat, extended cue, in order to support spatially tuned firing. This is in contrast to previous modeling work,[13,15,28] which suggested that flat boundaries could stabilize spatial cells, and the experimental finding that boundary-tuned neurons responded to flat "drop-off" boundaries.[29] Previous modeling work[13,15] and experimental virtual reality studies[16] have also emphasized the importance of optic flow from patterned visual cues in stabilizing spatial firing. However, our data show that, when only visual cues are available to the animal, optic flow from a patterned floor, although detected by place cells, is neither necessary nor sufficient to support stable place and grid cell firing.

Grid cell networks display conserved internal dynamics across behavioral states,[2,30,31] and when recorded in the absence of visual input, grid cells maintain consistent co-activity patterns,

Please cite this article in press as: Yang et al., Visual boundary cues suffice to anchor place and grid cells in virtual reality, Current Biology (2024), https://doi.org/10.1016/j.cub.2024.04.026

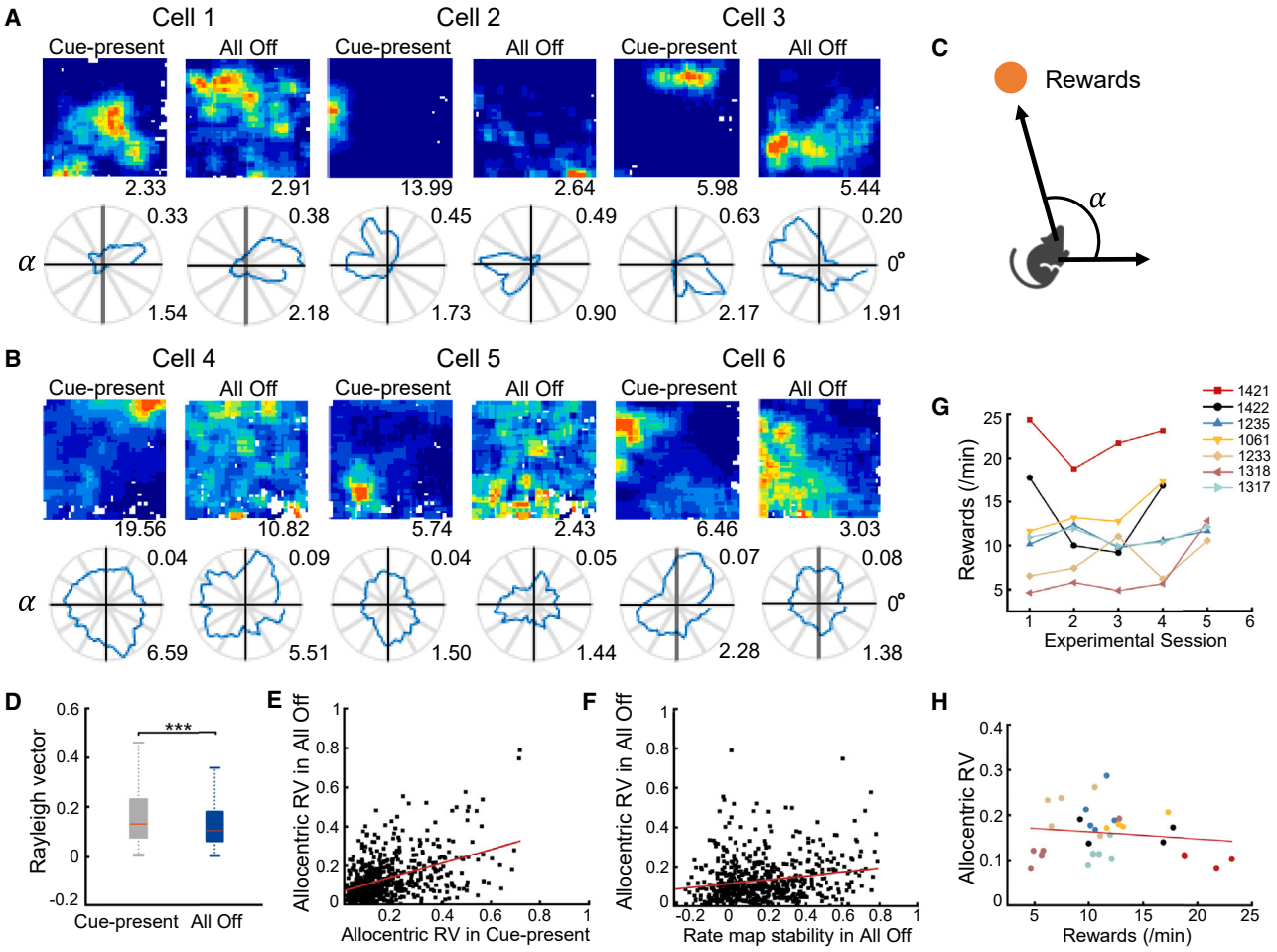

Figure 4. Place cell response to the locations of reward beacons

(A) Three example place cells showing strong directional tuning toward the location of reward beacons. The upper row shows 2D firing rate maps and the bottom row shows allocentric reward-bearing polar plots. Numbers at the bottom right of firing rate maps are peak firing rate (Hz). The numbers at the top right of polar plots are Rayleigh vector (RV) scores and the numbers at the bottom right are peak firing rates (Hz). Zero degrees marked on the polar plots (east) indicate the direction in which rewards are located.

(B) Three example place cells showing low Rayleigh vector scores. Format of data as for (A).

(C) Illustration of allocentric (α) direction relative to the location of a reward beacon.

(D) Rayleigh vector scores of allocentric tuning directions in the cue-present and all-off conditions. Red lines are median, blue boxes cover the interquartile range $q1-q3$, and dashed lines cover $q1 - 1.5 \times$ IQR to $q3 + 1.5 \times$ IQR including all data points. Cue-present, median = 0.12, IQR = 0.15; all-off, median = 0.10, IQR = 0.12 for allocentric RV scores, Wilcoxon rank-sum test, z = 7.30, $p < 0.001$. ***$p < 0.001$.

(E) Relationship of allocentric Rayleigh vectors between the cue-present and all-off conditions. Partial correlation, r = 0.44; $p < 0.001$, controlling for the boundary index.

(F) Relationship between the allocentric Rayleigh vectors and the intra-trial stability of rate maps in the all-off condition. Partial correlation, r = 0.19; $p < 0.001$, controlling for the boundary index.

(G) Number of rewards collected in each experimental session for all recorded mice. The number of rewards collected was measured in the cue-present condition.

(H) There is no significant correlation between the average allocentric RV values of place cell reward tuning and the number of rewards collected in the cue-present condition ($r = -0.14$, $p = 0.460$). Each dot represents one experimental session.

See also Figure S4.

despite spatial instability.[32] Our results suggest that grid cell instability may be caused by excessive accumulation of path integration error, such that the internally coherent grid network "drifts" with respect to the external world. This interpretation predicts that hexagonal grid patterns should be detectable at sufficiently short timescales, with the timescale depending on the rate of error accumulation. In contrast to the previous studies where only distance tuning, not drifting hexagonal patterns, could be detected when grid cell firing was disrupted in the dark,[32,33] our study is the first to demonstrate the presence of coherent but drifting hexagonal grid cell firing during spatial exploration and shows that, in our experimental setup, error accumulation begins to degrade grid stability from 5 s onward. Surprisingly, the presence of patterned visual cues on the floor

of the virtual environment does not reduce the rate of error accumulation, indicating that not all visual cues can stabilize grid firing equally and reinforcing the privileged role that boundaries play.

In addition to this, and unexpectedly, we observe that the firing patterns of place cells are more stable in areas near environmental boundaries even in the all-off condition, when the boundaries are not directly visible, and the only visible environmental cue available is the (moving) reward beacon. We therefore hypothesize that the animal can infer the presence of the boundary from the movement of the beacon, relative to the animal's own motor output. As the animal's progress through the virtual space is blocked when it encounters the invisible boundary, this creates a mismatch between the visually observed beacon movement and that predicted from the animal's own motor output. We hypothesize that the animal can use this mismatch to infer boundary position, such that this inferred boundary can enhance place cell stability. To our knowledge, this is the first demonstration that an "invisible" boundary, whose only physical manifestation is an impediment to movement, can modulate hippocampal spatial responses. Our results therefore expand the functional definition of boundaries to encompass entities that are not solely defined by their sensory characteristics.

A further unexpected aspect of our results was that grid cell fields are less stable close to boundaries in the presence of the full set of cues, in both virtual reality and real-world conditions. This result is seemingly in contrast with a previous report of enhanced grid cell stability following boundary contact,[8] though differences in environment size and methodology for assessing stability may explain the discrepancies between the two studies.

We observed a dissociation between the behavior of HDCs and that of place and grid cells, namely, only the former are stable in the walls-off and all-off conditions. Furthermore, unstable grids retain their orientations at short timescales, despite drifting translationally. These findings are consistent with previous real-world studies[32] and suggest a key functional dissociation between the robustness of directional and 2D spatial signals, under cue impoverished conditions. In this study, we cannot determine whether the cues stabilizing HDCs derive from virtual reality (e.g., reward beacon) or the real world (e.g., virtual reality projection monitors). A virtual landmark can control HDC preferred firing directions in our apparatus[9] (at least for rotations not in conflict with apparatus symmetry): future experiments could investigate further the effect of dissociating real and virtual reality cues, for example, through gradual rotations of virtual landmarks.

We showed that a subpopulation of place cells tracks the allocentric bearing of the animal to the reward beacon (which moves approximately every 4–5 s but is stable between these relocations). This result is consistent with the previously reported modulation of hippocampal place cell firing by (stable) goals and/or objects.[4,34–40] We observe a significant correlation between place cell stability and the degree of their allocentric directional tuning to the reward beacon, indicating that tracking the allocentric location of the visible reward beacon enhances place cell stability.

In this study, we used virtual reality to dissect the exact role and nature of visual cues that support spatially tuned firing. Although virtual reality cannot replicate all aspects of the real sensory environment (for example, olfactory cues[41,42]), findings obtained in virtual reality can nevertheless generalize to the real world. For example, human children tested on the spatial reorientation task[43] could not use the flat outline of a rectangle as a geometric reorientation cue,[44] consistent with the lack of spatial neuron stability in the walls-off environment observed in virtual reality.

STAR★METHODS

Detailed methods are provided in the online version of this paper and include the following:

- KEY RESOURCES TABLE
- RESOURCE AVAILABILITY
  - Lead contact
  - Materials availability
  - Data and code availability
- EXPERIMENTAL MODEL AND STUDY PARTICIPANT DETAILS
  - Experimental model
- METHOD DETAILS
  - Subjects and surgery
  - Virtual reality
  - Behavioral training
  - Cue manipulations
  - Real-world cell recordings
  - Data acquisition
- QUANTIFICATION AND STATISTICAL ANALYSIS
  - Classification of place cells and grid cells
  - Spike-triggered time-windowed rate maps
  - Place/grid field stability
  - Analysis of reward-modulated firing
  - Partial correlation

SUPPLEMENTAL INFORMATION

Supplemental information can be found online at https://doi.org/10.1016/j.cub.2024.04.026.

ACKNOWLEDGMENTS

This study was funded by the BBSRC (BB/W007878/1 to G.C. and BB/I021221/1 to F.C.), the Royal Society (RGS\R1\221070 and IEC\NSFC\233779 to G.C.), the European Union H2020 research and innovation programme (Human Brain Project #785907, SGA2 to G.C., F.C., and N.B.), China Scholarship Council (CSC202104910128 to X.Y. and G.C.), the Wellcome Trust (fellowship 220886/Z/20/Z to T.J.W.), the European Research Council (consolidator award "DEVMEM" to F.C.), and the Wellcome Trust (Investigator Award, 210690/Z/18/Z). We would also like to thank Dr. Daniel Manson for data analysis.

AUTHOR CONTRIBUTIONS

G.C. and F.C. conceived the study. G.C. and N.B. constructed and implemented the virtual reality setup. G.C. conducted the experiments and spike-sorted the data. X.Y., G.C., and T.J.W. analyzed the data. T.J.W., G.C., and F.C. wrote the manuscript with input from N.B.

DECLARATION OF INTERESTS

The authors declare no competing interests.

Received: October 17, 2023
Revised: March 1, 2024
Accepted: April 10, 2024
Published: May 2, 2024

REFERENCES

1. Burgess, N., and O'Keefe, J. (2011). Models of place and grid cell firing and theta rhythmicity. Curr. Opin. Neurobiol. *21*, 734–744. https://doi.org/10.1016/j.conb.2011.07.002.
2. Gardner, R.J., Hermansen, E., Pachitariu, M., Burak, Y., Baas, N.A., Dunn, B.A., Moser, M.-B., and Moser, E.I. (2022). Toroidal topology of population activity in grid cells. Nature *602*, 123–128. https://doi.org/10.1038/s41586-021-04268-7.
3. Dudchenko, P.A., Wood, E.R., and Smith, A. (2019). A new perspective on the head direction cell system and spatial behavior. Neurosci. Biobehav. Rev. *105*, 24–33. https://doi.org/10.1016/j.neubiorev.2019.06.036.
4. Gothard, K.M., Skaggs, W.E., Moore, K.M., and McNaughton, B.L. (1996). Binding of hippocampal CA1 neural activity to multiple reference frames in a landmark-based navigation task. J. Neurosci. *16*, 823–835. https://doi.org/10.1523/jneurosci.16-02-00823.1996.
5. Chen, G., Lu, Y., King, J.A., Cacucci, F., and Burgess, N. (2019). Differential influences of environment and self-motion on place and grid cell firing. Nat. Commun. *10*, 630. https://doi.org/10.1038/s41467-019-08550-1.
6. O'Keefe, J., and Burgess, N. (1996). Geometric determinants of the place fields of hippocampal neurons. Nature *381*, 425–428. https://doi.org/10.1038/381425a0.
7. Barry, C., Lever, C., Hayman, R., Hartley, T., Burton, S., O'Keefe, J., Jeffery, K., and Burgess, N. (2006). The boundary vector cell model of place cell firing and spatial memory. Rev. Neurosci. *17*, 71–97. https://doi.org/10.1515/revneuro.2006.17.1-2.71.
8. Hardcastle, K., Ganguli, S., and Giocomo, L.M. (2015). Environmental boundaries as an error correction mechanism for grid cells. Neuron *86*, 827–839. https://doi.org/10.1016/j.neuron.2015.03.039.
9. Chen, G., King, J.A., Lu, Y., Cacucci, F., and Burgess, N. (2018). Spatial cell firing during virtual navigation of open arenas by head-restrained mice. eLife *7*, e34789. https://doi.org/10.7554/elife.34789.
10. Burak, Y., and Fiete, I.R. (2009). Accurate path integration in continuous attractor network models of grid cells. PLoS Comput. Biol. *5*, e1000291. https://doi.org/10.1371/journal.pcbi.1000291.
11. Mhatre, H., Gorchetchnikov, A., and Grossberg, S. (2012). Grid cell hexagonal patterns formed by fast self-organized learning within entorhinal cortex. Hippocampus *22*, 320–334. https://doi.org/10.1002/hipo.20901.
12. Couey, J.J., Witoelar, A., Zhang, S.-J., Zheng, K., Ye, J., Dunn, B., Czajkowski, R., Moser, M.-B., Moser, E.I., Roudi, Y., and Witter, M.P. (2013). Recurrent inhibitory circuitry as a mechanism for grid formation. Nat. Neurosci. *16*, 318–324. https://doi.org/10.1038/nn.3310.
13. Raudies, F., and Hasselmo, M.E. (2015). Differences in visual-spatial input may underlie different compression properties of firing fields for grid cell modules in medial entorhinal cortex. PLoS Comput. Biol. *11*, e1004596. https://doi.org/10.1371/journal.pcbi.1004596.
14. Giocomo, L.M., Moser, M.-B., and Moser, E.I. (2011). Computational models of grid cells. Neuron *71*, 589–603. https://doi.org/10.1016/j.neuron.2011.07.023.
15. Raudies, F., Hinman, J.R., and Hasselmo, M.E. (2016). Modelling effects on grid cells of sensory input during self-motion. J. Physiol. *594*, 6513–6526. https://doi.org/10.1113/jp270649.
16. Campbell, M.G., Ocko, S.A., Mallory, C.S., Low, I.I.C., Ganguli, S., and Giocomo, L.M. (2018). Principles governing the integration of landmark and self-motion cues in entorhinal cortical codes for navigation. Nat. Neurosci. *21*, 1096–1106. https://doi.org/10.1038/s41593-018-0189-y.
17. O'Keefe, J., and Conway, D.H. (1978). Hippocampal place units in the freely moving rat: Why they fire where they fire. Exp. Brain Res. *31*, 573–590. https://doi.org/10.1007/bf00239813.
18. Poucet, B., Sargolini, F., Song, E.Y., Hangya, B., Fox, S., and Muller, R.U. (2014). Independence of landmark and self-motion-guided navigation: a different role for grid cells. Philos. Trans. R. Soc. Lond. B Biol. Sci. *369*, 20130370. https://doi.org/10.1098/rstb.2013.0370.
19. Save, E., Cressant, A., Thinus-Blanc, C., and Poucet, B. (1998). Spatial firing of hippocampal place cells in blind rats. J. Neurosci. *18*, 1818–1826. https://doi.org/10.1523/jneurosci.18-05-01818.1998.
20. Wood, E.R., Dudchenko, P.A., and Eichenbaum, H. (1999). The global record of memory in hippocampal neuronal activity. Nature *397*, 613–616. https://doi.org/10.1038/17605.
21. Gothard, K.M., Skaggs, W.E., and McNaughton, B.L. (1996). Dynamics of mismatch correction in the hippocampal ensemble code for space: interaction between path integration and environmental cues. J. Neurosci. *16*, 8027–8040. https://doi.org/10.1523/jneurosci.16-24-08027.1996.
22. Li, Y., Xu, J., Liu, Y., Zhu, J., Liu, N., Zeng, W., Huang, N., Rasch, M.J., Jiang, H., Gu, X., et al. (2017). A distinct entorhinal cortex to hippocampal CA1 direct circuit for olfactory associative learning. Nat. Neurosci. *20*, 559–570. https://doi.org/10.1038/nn.4517.
23. Haas, O.V., Henke, J., Leibold, C., and Thurley, K. (2019). Modality-specific subpopulations of place fields coexist in the hippocampus. Cereb. Cortex *29*, 1109–1120. https://doi.org/10.1093/cercor/bhy017.
24. Aronov, D., and Tank, D.W. (2014). Engagement of neural circuits underlying 2D spatial navigation in a rodent virtual reality system. Neuron *84*, 442–456. https://doi.org/10.1016/j.neuron.2014.08.042.
25. Savelli, F., Yoganarasimha, D., and Knierim, J.J. (2008). Influence of boundary removal on the spatial representations of the medial entorhinal cortex. Hippocampus *18*, 1270–1282. https://doi.org/10.1002/hipo.20511.
26. Stensola, T., Stensola, H., Moser, M.-B., and Moser, E.I. (2015). Shearing-induced asymmetry in entorhinal grid cells. Nature *518*, 207–212. https://doi.org/10.1038/nature14151.
27. Stangl, M., Topalovic, U., Inman, C.S., Hiller, S., Villaroman, D., Aghajan, Z.M., Christov-Moore, L., Hasulak, N.R., Rao, V.R., Halpern, C.H., et al. (2021). Boundary-anchored neural mechanisms of location-encoding for self and others. Nature *589*, 420–425. https://doi.org/10.1038/s41586-020-03073-y.
28. Raudies, F., and Hasselmo, M.E. (2012). Modeling boundary vector cell firing given optic flow as a cue. PLoS Comput. Biol. *8*, e1002553. https://doi.org/10.1371/journal.pcbi.1002553.
29. Stewart, S., Jeewajee, A., Wills, T.J., Burgess, N., and Lever, C. (2014). Boundary coding in the rat subiculum. Philos. Trans. R. Soc. Lond. B Biol. Sci. *369*, 20120514. https://doi.org/10.1098/rstb.2012.0514.
30. Trettel, S.G., Trimper, J.B., Hwaun, E., Fiete, I.R., and Colgin, L.L. (2019). Grid cell co-activity patterns during sleep reflect spatial overlap of grid fields during active behaviors. Nat. Neurosci. *22*, 609–617. https://doi.org/10.1038/s41593-019-0359-6.
31. Waaga, T., Agmon, H., Normand, V.A., Nagelhus, A., Gardner, R.J., Moser, M.-B., Moser, E.I., and Burak, Y. (2022). Grid-cell modules remain coordinated when neural activity is dissociated from external sensory cues. Neuron *110*, 1843–1856.e6. https://doi.org/10.1016/j.neuron.2022.03.011.
32. Chen, G., Manson, D., Cacucci, F., and Wills, T.J. (2016). Absence of visual input results in the disruption of grid cell firing in the mouse. Curr. Biol. *26*, 2335–2342. https://doi.org/10.1016/j.cub.2016.06.043.
33. Pérez-Escobar, J.A., Kornienko, O., Latuske, P., Kohler, L., and Allen, K. (2016). Visual landmarks sharpen grid cell metric and confer context specificity to neurons of the medial entorhinal cortex. eLife *5*, e16937. https://doi.org/10.7554/elife.16937.
34. Hollup, S.A., Molden, S., Donnett, J.G., Moser, M.-B., and Moser, E.I. (2001). Accumulation of hippocampal place fields at the goal location in an annular watermaze task. J. Neurosci. *21*, 1635–1644. https://doi.org/10.1523/jneurosci.21-05-01635.2001.
35. Jazi, M.N., Tymorek, A., Yen, T.-Y., Kavarayil, F.J., Stingl, M., Chau, S.R., Baskurt, B., Vilela, C.G., and Allen, K. (2022). Hippocampal firing fields anchored to a moving object predict homing direction during path-integration-based behavior. Preprint at bioRxiv. https://doi.org/10.1101/2022.09.30.510268.

36. Hok, V., Lenck-Santini, P.-P., Roux, S., Save, E., Muller, R.U., and Poucet, B. (2007). Goal-related activity in hippocampal place cells. J. Neurosci. *27*, 472–482. https://doi.org/10.1523/jneurosci.2864-06.2007.

37. Sarel, A., Finkelstein, A., Las, L., and Ulanovsky, N. (2017). Vectorial representation of spatial goals in the hippocampus of bats. Science *355*, 176–180. https://doi.org/10.1126/science.aak9589.

38. Ormond, J., and O'Keefe, J. (2022). Hippocampal place cells have goal-oriented vector fields during navigation. Nature *607*, 741–746. https://doi.org/10.1038/s41586-022-04913-9.

39. Nagelhus, A., Andersson, S.O., Cogno, S.G., Moser, E.I., and Moser, M.-B. (2023). Object-centered population coding in CA1 of the hippocampus. Neuron *111*, 2091–2104.e14. https://doi.org/10.1016/j.neuron.2023.04.008.

40. Vandrey, B., Duncan, S., and Ainge, J.A. (2021). Object and object-memory representations across the proximodistal axis of CA1. Hippocampus *31*, 881–896. https://doi.org/10.1002/hipo.23331.

41. Zhang, S., and Manahan-Vaughan, D. (2015). Spatial olfactory learning contributes to place field formation in the hippocampus. Cereb. Cortex *25*, 423–432. https://doi.org/10.1093/cercor/bht239.

42. Radvansky, B.A., and Dombeck, D.A. (2018). An olfactory virtual reality system for mice. Nat. Commun. *9*, 839. https://doi.org/10.1038/s41467-018-03262-4.

43. Hermer, L., and Spelke, E. (1996). Modularity and development: the case of spatial reorientation. Cognition *61*, 195–232. https://doi.org/10.1016/s0010-0277(96)00714-7.

44. Lee, S.A., and Spelke, E.S. (2011). Young children reorient by computing layout geometry, not by matching images of the environment. Psychon. Bull. Rev. *18*, 192–198. https://doi.org/10.3758/s13423-010-0035-z.

45. Bonnevie, T., Dunn, B., Fyhn, M., Hafting, T., Derdikman, D., Kubie, J.L., Roudi, Y., Moser, E.I., and Moser, M.-B. (2013). Grid cells require excitatory drive from the hippocampus. Nat. Neurosci. *16*, 309–317. https://doi.org/10.1038/nn.3311.

46. Brandon, M.P., Bogaard, A.R., Libby, C.P., Connerney, M.A., Gupta, K., and Hasselmo, M.E. (2011). Reduction of theta rhythm dissociates grid cell spatial periodicity from directional tuning. Science *332*, 595–599. https://doi.org/10.1126/science.1201652.

Please cite this article in press as: Yang et al., Visual boundary cues suffice to anchor place and grid cells in virtual reality, Current Biology (2024), https://doi.org/10.1016/j.cub.2024.04.026

STAR★METHODS

KEY RESOURCES TABLE

REAGENT or RESOURCE	SOURCE	IDENTIFIER
Deposited data		
Data	https://osf.io/m8qwp/	N/A
Experimental models: Organisms/strains		
Mice	Charles River	C57BL/6
Software and algorithms		
Unity	https://unity.com/	N/A
SPSS	https://www.ibm.com/products/spss-statistics	RRID: SCR_002865
MATLAB	https://uk.mathworks.com/products/matlab.html	RRID: SCR_001622

RESOURCE AVAILABILITY

Lead contact

Further information and requests for resources and reagents should be directed to and will be fulfilled by the lead contact, Guifen Chen (guifen.chen@qmul.ac.uk).

Materials availability

This study did not generate new unique reagents.

Data and code availability

- There are no standardized datatypes generated in this study. Data reported in this paper is shared on https://osf.io/m8qwp/.
- This paper does not report the original code.
- Any additional information required to reanalyze the data reported in this paper is available from the lead contact upon request.

EXPERIMENTAL MODEL AND STUDY PARTICIPANT DETAILS

Experimental model

Seven male 3-month-old C57BL/6 mice were used and housed under a reversed 12h/12h light/dark cycle (lights on at 10 a.m.).

METHOD DETAILS

Subjects and surgery

Mice were implanted with custom-made head plates and microdrives loaded with 17μm platinum-iridium tetrodes. Each mouse received a dual implant with one microdrive in right CA1 (ML: 1.8 mm, AP: 2.1 mm posterior to bregma) and the other in left mEC (ML = 3.1 mm, AP = 0.2 mm anterior to the transverse sinus, angled 4° posteriorly), each drive carrying four tetrodes. See further details in Chen et al.[5] All procedures were carried out under the Animals (Scientific Procedures) Act 1986.

Virtual reality

Virtual environments (Figure S1A) were constructed using a game engine (Unity, Unity Technologies) which ran on a Dell Precision T7500 workstation. The virtual scenes were rendered on a combination of four Acer B236HL LCD monitors mounted vertically in a square array plus two LCD projectors (native resolution 480 × 320, 150 lumens) mounted above. A mouse was attached to a head holder mounted in a bearing (Kaydon Reali-Slim bearing KA020XP0), which allowed free rotation on the horizontal plane. The bearing was held over the centre of an air-supported 200mm-diameter hollow polystyrene ball. The movement of the ball, triggered by the movement of the animal, can be detected by two optical computer mice (Logitech G700s gaming mouse) mounted with orthogonal orientations at the front and side of the ball. The output of the two optical mice drove the translational movement of the virtual scene in the X and Y axes respectively, corresponding to the movement of the animal.[5,9] When the animal reached the edge of the virtual environment, the ball could continue to move freely, but the animal's position within the virtual environment remained at the boundary, until the animal moved away from the wall. The virtual reality environment included realistic parallax, such that visual stimuli for near objects move faster than visual stimuli for far objects, given a constant mouse speed.

Please cite this article in press as: Yang et al., Visual boundary cues suffice to anchor place and grid cells in virtual reality, Current Biology (2024), https://doi.org/10.1016/j.cub.2024.04.026

CellPress
OPEN ACCESS

Behavioral training

After recovery from surgery, mice were also exposed to a 60 cm × 60 cm square in a real environment to screen for place cells and grid cells. Electrodes were lowered by 62.5 μm per day independently on each side of the hemisphere until the spatial cells were found. In the meantime, mice were trained in the virtual environments as presented in Chen et al.,[5,9] learning to forage for the rewards indicated by a visual beacon. Foraging behavior was motivated by sweetened soya milk drops as a reward, delivered through a tube positioned within licking distance of the animal's mouth. Visual beacons (a striped cylinder and a black rounded disk, see Figure S1A) were placed in the virtual environments randomly to indicate the reward locations. At any given moment, there was always one reward location visually indicated by the beacon. The beacon would remain at the same location until mice visited the virtual rewarded location, at which point a drop of milk would be delivered. Once the reward was delivered, the beacon would be repositioned to a different random location, which could be at any position within the virtual environment, except within a radius of 20cm from the previous reward position.

Cue manipulations

A typical experimental session comprised two 40-min trials with a 40-min interval. Each trial consisted of either 40-min baseline trial or 20-min baseline and a 20-min manipulation trial. In the baseline trial - 'Cue-present', animals forage for rewards in a familiar 60 cm × 60 cm virtual square environment identical to the one used during training. In the manipulation trial - 'Cue-absent', subsets of the visible cues in the virtual square environment were removed and replaced with a dark grey background (Figure S1A). There were three types of manipulations: Floor-Off, Walls-Off and All-Off. In the Floor-Off condition, the patterned floor texture was substituted with a plain grey area, while animals maintained physical contact with the ball. In the Walls-Off condition, both distal and proximal wall textures were replaced with a plain grey background. In the All-Off condition, the only visible virtual cue was the reward beacon: all other VR stimuli were replaced with a plain grey surface. The visual reward beacons were still available to indicate the location of reward, in all 'Cue-absent' trials. They moved to a pseudo-random location after the mouse had consumed the reward. Notably, the movement of the animal was restricted to within the same environment boundaries in all manipulation conditions, hence the animal's movement within the virtual arena would cease if it ran into a boundary, which could be detected even in the All-Off condition by a lack of corresponding movement of the reward beacon. On average, the reward beacon moved approximately every 4-5 s, but was stable between these relocations.

On any given day, one manipulation and at least one baseline trial where all visual cues were present (a 'Cue-present' trial, see Figure S1A) were carried out.

Real-world cell recordings

Using the same cohort of animals as for the VR experiments, 20-min recordings were carried out in a real-world open-field environment. The environment was a square, 60cm side length, walls were 50cm high. All walls were constructed from wood painted plain light grey covered with a similar patterned texture used in the VR. The floor was black perspex. Extra maze cues consisted of a prominent white cue card (A0, 84 cm × 119 cm), illuminated by a lamp. Animals were encouraged to forage for randomly scattered rewards on condensed milk. The floor was washed to scramble/minimize olfactory cues before each trial.

Data acquisition

Extracellular action potentials were recorded using DACQ (Axona Ltd., UK). Spike sorting was performed offline using an automated clustering algorithm (KlustaKwik) followed by a manual review and editing step using an interactive graphical tool 'Waveform' (https://github.com/d1manson/waveform).

QUANTIFICATION AND STATISTICAL ANALYSIS

Classification of place cells and grid cells

Firing rate maps were constructed using 1.5 × 1.5 cm bins and a 5 × 5 boxcar filter. Spatial information and gridness scores were calculated using the methods in Chen et al.[32] Cells were classified as grid cells if their gridness scores in a Cue-present condition exceeded the 95th percentile of a distribution of 1,000 gridness scores derived from spatially shuffled data, created by temporally shifting the spike train relative to position. Place cells were defined in a similar fashion, with spatial information being used to quantify the spatial tuning of a neuron.

Spike-triggered time-windowed rate maps

Time-windowed spatial displacement rate maps were constructed following the methods in Bonnevie et al.[45] In detail, the spike times of one neuron (the 'reference' neuron) were used to define a series of time windows of duration T seconds, each starting at the time of a reference neuron spike. Windows were reduced in duration if a reference spike occurred within T seconds of the end of the trial. The position at the time of the reference neuron spike was assigned an (x,y) value of (0,0). Within each time window, a 2-dimensional histogram was created of the (x,y) positions associated with the spiking of the second neuron (the 'test' neuron; bin size = 1.5 cm), with positions being defined relative to that at the time of the reference neuron spike. The histograms of all windows were then summed, and smoothed, producing an overall map of the positions in which the test neuron fired relative to the reference neuron, within a short time window. To control for uneven patterns of movement, the spike histogram was then divided by a summed, smoothed, histogram

Please cite this article in press as: Yang et al., Visual boundary cues suffice to anchor place and grid cells in virtual reality, Current Biology (2024), https://doi.org/10.1016/j.cub.2024.04.026

of all of the relative dwell times across all time windows: this defined the spatial cross-correlogram. The values of T were set to 2, 5, 10, 20, 40 and 80 s. Cross-cell time-windowed maps ('time-windowed cross-correlograms') were constructed in an analogous fashion, except that the reference spike times were taken from one grid cell, and the test spike times were taken from another, simultaneously recorded, grid cell. Within each pair of grid cells, Cell A and Cell B, time-windowed rate-maps were generated using both Cell A as reference and Cell B as Test, and Cell B as reference and Cell A as Test. Following this, the spatial cross-correlogram between the two time-windowed rate maps was calculated, to provide a more accurate estimate of the directional offset between the two grid patterns. Within a simultaneously recorded ensemble, all possible grid cell pairs combinations were used for the analysis, with the sole restriction that a grid cell could only contribute if its time-windowed auto-correlogram gridness score was >0.17 (at a 10 s time window). We introduced this threshold to ensure that only well-sampled cross-correlograms were used. The value of the threshold was derived from a population of gridnesses of spike-time shuffled auto-correlograms in the All-Off condition at the 95% percentile.

The gridness scores for the time-windowed maps were calculated by taking maximum gridness scores computed from rings as described as 'Gridness measure 2'.[46] In brief, an autocorrelation of a smoothed rate map was first calculated and seven peaks closest to the center were identified. The inner radius of the ring was defined as half of the mean distance from the peaks to the center, and the outer radii ranged from the inner radius to the closest autocorrelogram edge. Then the rotational autocorrelations of these rings were calculated and a set of gridness scores were computed as the difference between the lowest correlation observed at 60 or 120 degrees of rotation and the highest correlation at 30, 90, or 150°.

Place/grid field stability

Intra-trial stability was calculated by correlating the firing rates of spatially corresponding bins between the first and the second halves of a trial. Inter-trial stability was measured by correlating the firing rates of spatially corresponding bins between the baseline and manipulation trials. To compare the field stability, the entire environment was divided equally into two zones: central and boundary. Central position bins were assigned to the central zone and surrounding position bins to the boundary zone, ensuring an equal number of bins in each zone.

Analysis of reward-modulated firing

Allocentric reward-bearing polar plots were constructed by first calculating, for every position sample, the angle to the current reward position in the virtual environment reference frame. Angles were then binned into 6° bins, and spikes assigned to each bin. Both position maps and spike maps were smoothed separately using a 30° wide boxcar filter and finally the smoothed spike maps were divided by the smoothed position maps. The directional tuning of the cell was measured using the length of the mean resultant vector (Rayleigh Vector; RV) of the bins of the reward-tuned directional firing rate maps. To classify cells as reward-tuned, the actual RV lengths were compared to null distributions of RV lengths derived from two different populations of spike-shuffled data, generated by: (1) shifting the entire spike train randomly with respect to position (as for place and grid cell classification), (2) maintaining the mean firing rate in each 2-dimensional rate map bin, but reassigning the spikes which occurred in each rate map bin randomly across the total set of time points for which the animal occupied that same bin. The second shuffle controlled for artifactual reward-bearing tunings which may have arisen primarily from the concentration of firing in one particular (2-dimensional) location. A cell was classified as reward-tuned if its reward-bearing map RV length exceeded the higher of the 99th percentiles of the two shuffled reward-bearing RV lengths described above.

To examine the reward tuning in two-dimensional space, a time window of 5 s was used to construct time-windowed rate maps centered around actual reward delivery times. The beacon-centered maps therefore effectively replot the spatial firing of neurons such that the upcoming reward beacon is always at (x,y) coordinate (0,0). Windows were truncated when the next reward was delivered in less than 5 s. To establish a negative control for comparison, time-windowed rate maps were also constructed using a shuffled set of reward positions, which was generated through a random re-ordering of the actual beacon positions used in a trial.

Partial correlation

To test whether the enhanced stability of reward-tuned cells was primarily driven by their proximity to a boundary, the correlation of stability versus reward tuning was a partial correlation, controlling for a 'boundary score', which quantified the extent to which firing occurred near a boundary. The boundary score was calculated by assigning weights to each bin in a rate map based on its distance to the closest edge. The boundary score for each cell was defined by the sum of the firing rates within each bin multiplied by the corresponding weight from the mask.